

Dirigent Protein-Mediated Lignan and Cyanogenic Glucoside Formation in Flax Seed: Integrated Omics and MALDI Mass Spectrometry Imaging

Doralyn S. Dalisay,[†] Kye Won Kim,[†] Choonseok Lee,[†] Hong Yang,[†] Oliver Rübel,[‡] Benjamin P. Bowen,[§] Laurence B. Davin,[†] and Norman G. Lewis^{*,†}

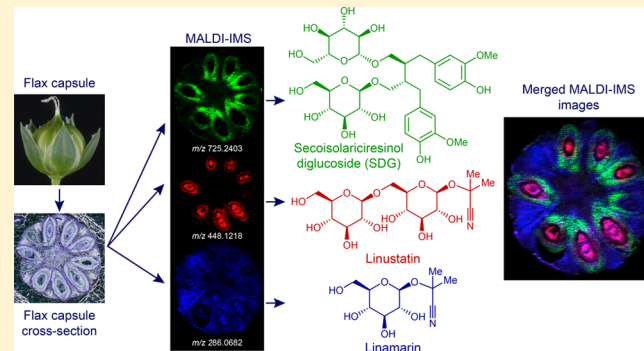
[†]Institute of Biological Chemistry, Washington State University, Pullman, Washington 99164-6340, United States

[‡]Computational Research Division, Lawrence Berkeley National Laboratory, One Cyclotron Road, Berkeley, California 94720, United States

[§]Life Sciences Division, Lawrence Berkeley National Laboratory, One Cyclotron Road, Berkeley, California 94720, United States

Supporting Information

ABSTRACT: An integrated omics approach using genomics, transcriptomics, metabolomics (MALDI mass spectrometry imaging, MSI), and bioinformatics was employed to study spatiotemporal formation and deposition of health-protecting polymeric lignans and plant defense cyanogenic glucosides. Intact flax (*Linum usitatissimum*) capsules and seed tissues at different development stages were analyzed. Transcriptome analyses indicated distinct expression patterns of dirigent protein (DP) gene family members encoding (−)- and (+)-pinoresinol-forming DPs and their associated downstream metabolic processes, respectively, with the former expressed at early seed coat development stages. Genes encoding (+)-pinoresinol-forming DPs were, in contrast, expressed at later development stages. Recombinant DP expression and DP assays also unequivocally established their distinct stereoselective biochemical functions. Using MALDI MSI and ion mobility separation analyses, the pinoresinol downstream derivatives, secoisolariciresinol diglucoside (SDG) and SDG hydroxymethylglutaryl ester, were localized and detectable only in early seed coat development stages. SDG derivatives were then converted into higher molecular weight phenolics during seed coat maturation. By contrast, the plant defense cyanogenic glucosides, the monoglucosides linamarin/lotaustralin, were detected throughout the flax capsule, whereas diglucosides linustatin/neolinustatin only accumulated in endosperm and embryo tissues. A putative biosynthetic pathway to the cyanogens is proposed on the basis of transcriptome coexpression data. Localization of all metabolites was at ca. 20 μm resolution, with the web based tool OpenMSI enabling not only resolution enhancement but also an interactive system for real-time searching for any ion in the tissue under analysis.



Flax (*Linum usitatissimum*) seeds accumulate high molecular weight phenolics (estimated to be ca. 4.3 kDa¹) that are mainly of mixed biochemical pathway (lignan- and hydroxymethylglutaryl CoA) origin.^{2,3} These solvent-extractable phenolics are largely derived from secoisolariciresinol diglucoside (SDG, 1, Figure 1A) covalently ester linked to hydroxymethylglutaric acid (HMG) moieties (e.g., 2 and 3). During seed maturation, the intermediary metabolic precursors 1–3 so formed are converted into the SDG-HMG derived oligomeric/polymeric end products.^{2,3} Mild alkali treatment of mature seed, however, results in facile release of SDG (1)² through ester group cleavage, with this latter substance being greatly valued in the nutraceutical industry.⁴ The SDG (1) released exists in two diastereomeric forms, with that derived from (+)-secoisolariciresinol (11a, Figure 1B) being predominant (~99%) relative to (−)-secoisolariciresinol (11b) (~1%).²

From our earlier work with flax and other species, it was established that (+)- and (−)-forms of secoisolariciresinol (11a and 11b) are derived *in planta* via distinctive stereoselective coupling of coniferyl alcohol (8) moieties (Figure 1B), with control over product stereochemistry resulting from mediation by two distinct dirigent proteins (DPS) to initially give either (+)- or (−)-pinoresinols (9a or 9b), respectively.^{5–10} Each pinoresinol antipode (9a or 9b) so generated can then be enantiospecifically reduced, through action of either enantioselective pinoresinol reductases (PRs) in *Arabidopsis thaliana*,¹¹ or enantiospecific pinoresinol-lariciresinol reductases (PLRs) in *Forsythia intermedia*,¹² flax seed,¹³ flax aerial tissues,¹⁴ and western red cedar (*Thuja plicata*).¹⁵ Yet, while DP assays with flax seed extracts incubated with coniferyl alcohol (8) resulted

Received: January 9, 2015

Published: May 17, 2015

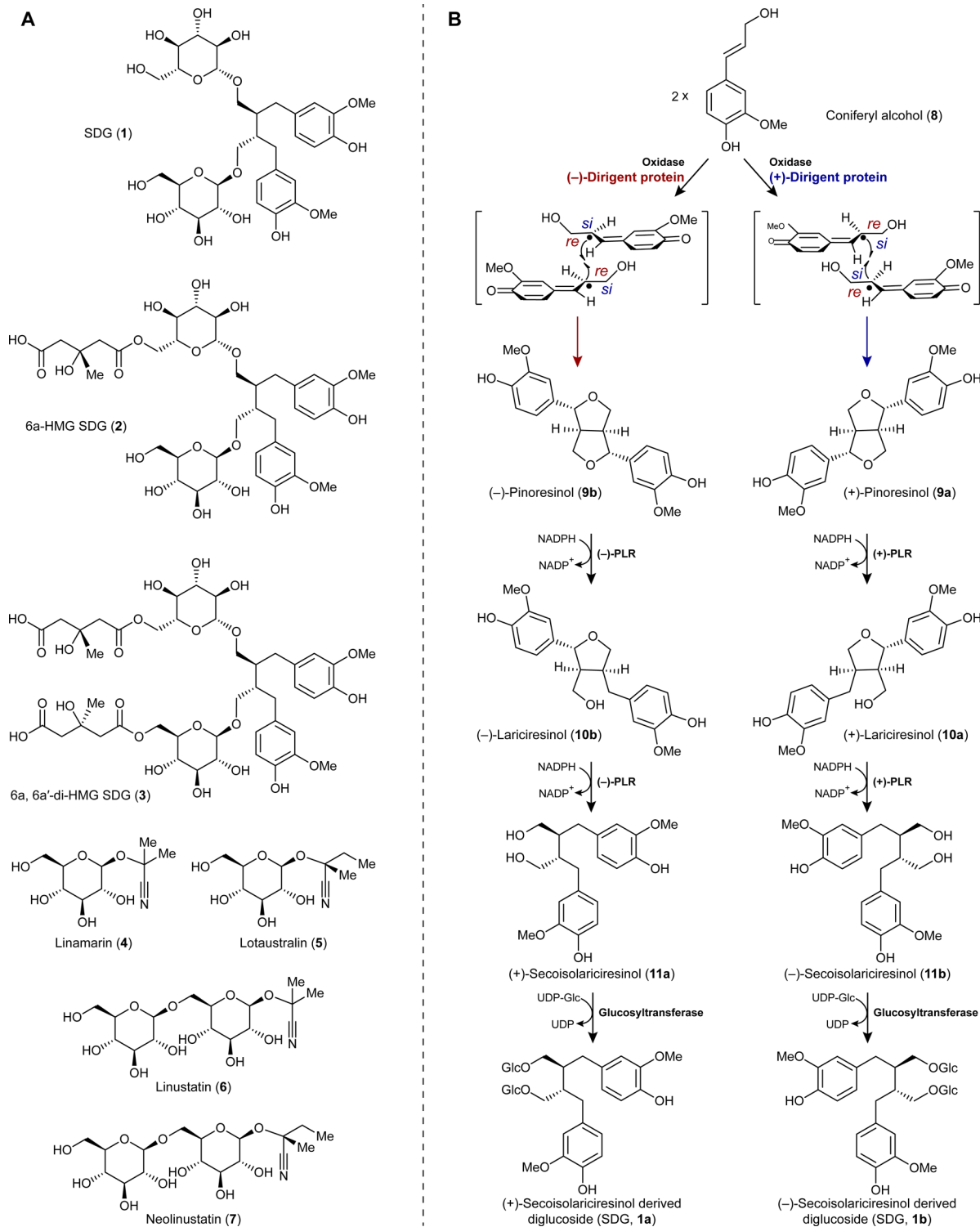


Figure 1. (A) Flax lignans (**1–3**) and cyanogenic glucosides (**4–7**). (B) Biochemical pathway to secoisolaricresinol diglucoside (SDG) (**1**).

in entry coupling step detection (i.e., to (−)-pinoresinol (**9b**) formation),^{16,17} attempts to isolate the (−)-pinoresinol-forming DP, as well as its encoding gene, failed. Instead, a PCR guided approach using degenerate primers only yielded a (+)-pinoresinol-forming DP.¹⁶

Herein, the genes encoding both (−)- and (+)-pinoresinol DPs from developing flax seed are reported, with matrix-assisted laser desorption/ionization (MALDI) mass spectrometry imaging (MSI) *in situ*^{10,18,19} employed to gain key insights

on metabolite localization during constitutive seed/seed coat development. In particular, application of the OpenMSI²⁰ web-based platform also enabled facile interactive analysis of raw data for metabolite imaging *in situ*. This included mapping localization in developing flax capsules of SDG (**1**) and HMG SDG derivative **2**, as well as the cyanogenic glucosides linamarin (**4**), lotaustralin (**5**), linustatin (**6**), and neolinustatin (**7**). The latter four metabolites are implicated in plant defense

as they can liberate HCN upon enzymatic hydrolysis during tissue disruption.^{21–23}

RESULTS AND DISCUSSION

In silico Flax Genome Analysis. With two distinct (+)- and (−)-stereoselective pinoresinol-forming DPs characterized from various plant species,^{5–10,24} a BLAST search of the complete flax genome sequence (var. CDC Bethune, <http://phytozome.org/>)²⁵ was performed, in order to tentatively identify the putative and elusive (−)-pinoresinol-forming DPs. Six potential (+)- and (−)-pinoresinol-forming DP homologues were thus provisionally annotated (Table 1 and Figure 2A),

Table 1. LuDIR Homologues

gene	<i>Linum usitatissimum</i>	GenBank number	identity with ScDIR (%)	identity with AtDIR6 (%)	size (a.a.)
<i>LuDIR1</i>	Lus10032331	KM433751	57.9	45.3	186
<i>LuDIR2</i>	Lus10024715	KM433754	58.4	45.3	186
<i>LuDIR3</i>	Lus10024714	KM433755	58.4	44.8	186
<i>LuDIR4</i>	Lus10017538	KM433756	66.1	45.8	169
<i>LuDIR5</i>	Lus10028749	KM433753	43.8	56.0	203
<i>LuDIR6</i>	Lus10017539	KM433752	45.4	57.1	196

these having 44–66% amino acid (a.a.) sequence identity to either the *Schizandra chinensis* (+)-pinoresinol-forming DP (*ScDIR*) or the corresponding *Arabidopsis thaliana* (−)-pinoresinol-forming DP (*AtDIR6*).⁶ The six *LuDIR* homologues were then divided into two distinctive groups on the basis of the highest a.a. sequence identity level to *ScDIR* or to *AtDIR6*: of these, *LuDIR1*–*LuDIR4* were ~58–66% identical to the (+)-pinoresinol-forming DP, *ScDIR*, and shared 94–96% identity with each other. The remaining two, *LuDIR5* and *LuDIR6*, showed ~56–57% amino acid sequence identity to the (−)-pinoresinol-forming DP, *AtDIR6*, with these being ~88% identical to each other. Overall, the identity/similarity levels between the flax (−)- and (+)-pinoresinol-forming DPs were 42–43%/60–62%, respectively.

Recombinant DP Expression and Biochemical Assays.

LuDIR5 and *LuDIR6* genes were obtained from flax genomic DNA by PCR amplification using gene-specific primers (Table S1 in the Supporting Information). Both were individually subcloned into the pART17 vector for recombinant DP expression⁶ in a tomato cell culture system.⁷ Recombinant *LuDIR5* and *LuDIR6* were then individually purified to apparent homogeneity using $(\text{NH}_4)_2\text{SO}_4$ fractionation and cation-exchange column chromatography,⁶ yielding 60 and 40 μg proteins, respectively, from nine liters of culture medium. To initially obtain the gene encoding *LuDIR1*,¹⁶ DNA sequences of (+)-pinoresinol-forming DPs from *Forsythia intermedia*,¹⁵ *Thuja plicata*,²⁴ and *Schizandra chinensis*²⁶ were compared, with degenerate primers (Table S1 in the Supporting Information) designed to PCR amplify the consensus region of the flax DP. Afterward, upstream and downstream regions were obtained by genome walking with the entire *LuDIR1* gene amplified from flax seed mRNA using the sequence information obtained above. For heterologous expression of recombinant *LuDIR1*, the pMT/VS-TOPO vector in insect (*Drosophila melanogaster* Schneider2) cells was used, with expression induced by copper sulfate,⁶ in a yield of ~400 μg from six liters of culture.

Purified recombinant *LuDIR1*, *LuDIR5*, and *LuDIR6* were individually assayed with assay mixtures each containing *Trametes versicolor* laccase (for one-electron oxidation) and substrate coniferyl alcohol (**8**) at various concentrations of recombinant *LuDIR* proteins. Assays with recombinant *LuDIR5* gave (−)-pinoresinol (**9b**, Figure 2B) formation in ~71% enantiomeric excess (ee) in the presence of 4.8 μM DP (Figure 2C), and similarly *LuDIR6* gave (−)-pinoresinol (**9b**, Figure 2B) in ~90% ee (4.8 μM DP, Figure 2C). *LuDIR1* was also further characterized as a (+)-pinoresinol-forming DP, engendering preferential formation of (+)-pinoresinol (**9a**) in ~43% ee with 16 μM protein, whereas doubling its concentration (32 μM) increased coupling stereoselectivity to ~69% ee (Figure 2D).

In situ Spatiotemporal Mapping of SDG (1) and SDG HMG (2) in Developing Flax Capsule and Seed Coat Tissues by MALDI MSI. MALDI mass spectrometry imaging (MSI) is a metabolomics-based approach that has been successfully employed *in planta* for mapping various natural products in tissues and subcellular compartments without aid of probes or antibodies.^{10,18,19} Herein, we wished to use MALDI MSI with time-of-flight (TOF) analyzer at high spatial/mass resolution to ascertain where and when the intermediary SDG (1) and its 6a-HMG-SDG (2) derivative² accumulate in developing flax seed, prior to their being subsequently converted into the aforementioned higher molecular weight phenolics. Thus, flax capsules (pods) were analyzed at different time points during seed/seed coat development.

With respect to flax capsule anatomy, the flax flower has five sepals, five petals, five stamens, and five fused carpels (each composed of an ovary, style, and stigma) (Figure 3A). The five carpels later produce round capsules 6–9 mm in diameter (Figure 3B), with each carpel having two distinct locules divided by a wall called a septum; the maximum number of seeds possible in a capsule is thus 10 (Figure 3C). In turn, each seed has an embryo (e), an endosperm (en), and a seed coat (Figure 3C), where the latter has two regions: inner integument containing a brown layer, and outer integument (testa) comprised of membraniform, sclerite cell and parenchymatous layers, as well as outermost mucilage cells (not shown).²⁷

In our analyses, MALDI MSI was combined with ion mobility separation (IMS) as a supplemental platform to analyze and differentiate ions by charge, size, and shape via their corresponding drift times. Accordingly, analyte identities *in situ* were determined via their accurate mass, ion mobility drift times (bins or milliseconds, ms), and through comparison to reference standards by IMS, collision-induced dissociation (CID), and data-dependent tandem mass spectrometry analysis (MS/MS), respectively. In preliminary experiments, it was established that a SDG (1) standard ionized as its potassium adduct m/z 725.2412 [$\text{M} + \text{K}$]⁺ (Δ ppm 1.5) using dihydroxybenzoic acid (DHB) as matrix (Figure 3D).

Next, flax capsules at 0 (day flower opens), 3, 4, 6, 7, 10, and 12 days after flowering (DAF) were analyzed. Under the conditions employed, SDG (1) was first detected in cross-sections of 6 and 7 DAF capsules from among the several hundred peaks visible in the MALDI-TOF imaging data. Specifically, its potassium adduct was detected at m/z 725.2452 [$\text{M} + \text{K}$]⁺ (Δ ppm 3.9) (Figure 3E) and m/z 725.2403 [$\text{M} + \text{K}$]⁺ (Δ ppm 2.7) (Figure S1 in the Supporting Information), respectively. Moreover, the IMS drift times of both standard and SDG (1) *in planta* were 102.28 (5.4754 ms) and 102.24 bins (5.4732 ms) (Figures 3F,G), providing further unequivocal

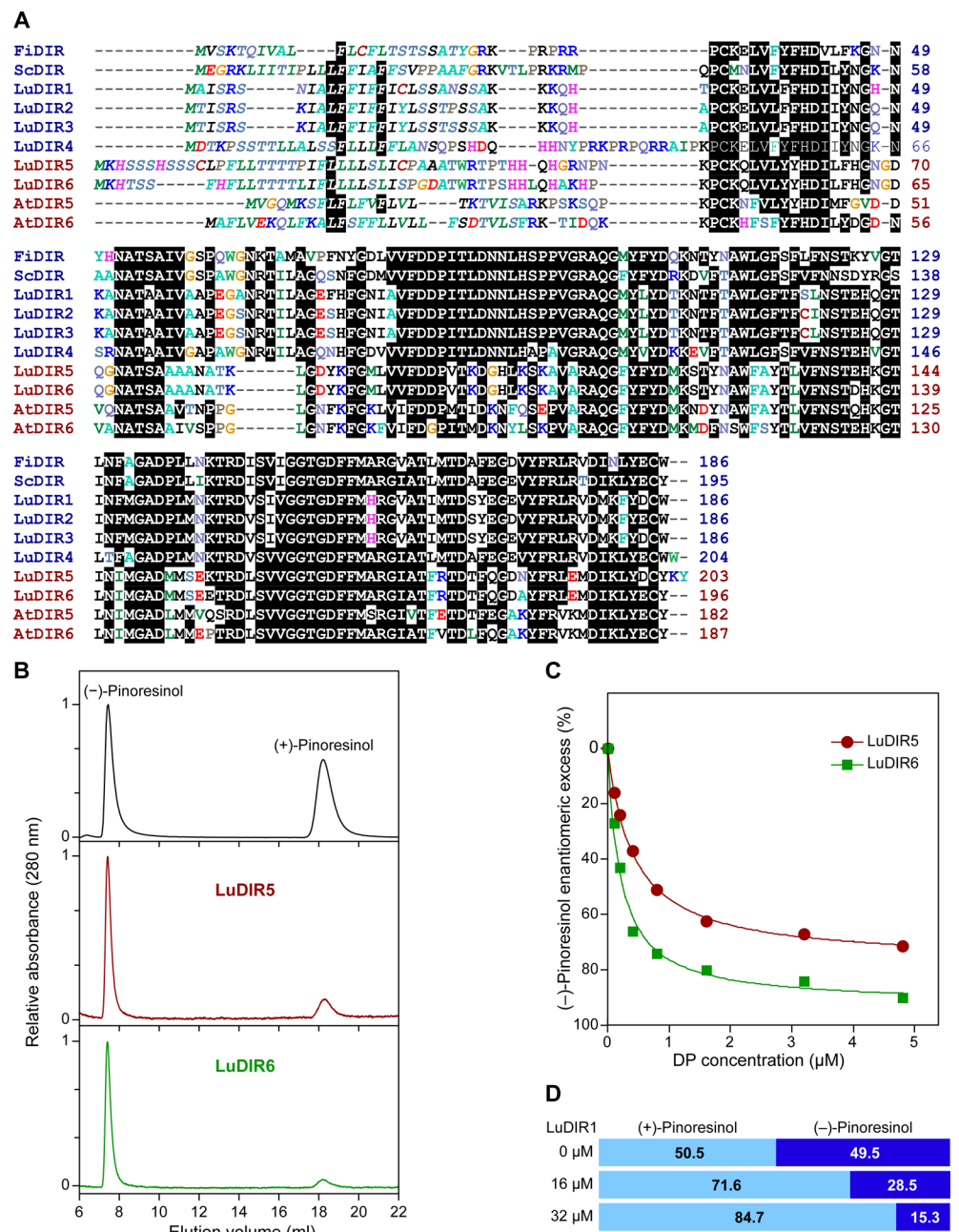


Figure 2. (A) Amino acid sequence comparison of LuDIR homologues (LuDIR1–LuDIR6) with (+)-pinoresinol-forming DPs (FiDIR and ScDIR) and (−)-pinoresinol-forming DPs (AtDIR5 and AtDIR6). Signal peptides were predicted with the SignalP 4.1 Server and are denoted in italic characters. At, *Arabidopsis thaliana*; Fi, *Forsythia intermedia*; Lu, *Linum usitatissimum*; Sc, *Schizandra chinensis*. (B–D) Differential stereoselectivity of distinct recombinant flax DPs. (B) Chiral HPLC analyses of authentic racemic (\pm)-pinoresinols (9a/9b, top panel), and pinoresinol (9a and 9b) products formed by recombinant LuDIR5 (4.8 μ M, middle panel) and LuDIR6 (4.8 μ M, bottom panel), respectively. (C) Enantiomeric excess (ee) of (−)-pinoresinol (9b) formation at various concentrations of recombinant LuDIR5 and LuDIR6. (D) Ratios of (+)- and (−)-pinoresinols (9a and 9b) formed using different concentrations of recombinant LuDIR1. In (C) and (D), each data point corresponds to a single independent measurement for each concentration tested. The experiments were repeated 4 times with similar results.

identification. CID MS/MS fragmentation of the detected $[M + K]^+$ ion also gave main fragmentation ions at m/z 401 for both the authentic standard and the detected SDG (1) in the flax seed tissue; however, different collision energies were required (40 eV for the standard vs 75 eV for detection in the tissue). Moreover, other ions were also detected, perhaps indicative of another component at m/z 725.23 undergoing fragmentation as well. It should also be emphasized that the SDG (1) in the seed coat was detected at a very low concentration.

6a-HMG-SDG (2) was also detected as a potassium adduct m/z 869.2892 $[M + K]^+$ (Δ ppm 5.2) and m/z 869.2818 $[M + K]^+$ (Δ ppm 3.2) in the plethora of metabolites (Figure 3E and Figure S1 in the Supporting Information). Neither SDG (1) nor 6a-HMG-SDG (2) were detected at later developmental/maturity stages (>7 DAF) due to their further conversion to higher molecular weight SDG-HMG containing phenolics. Conversely, the ions corresponding to pinoresinol (9) (m/z 397.1053 $[M + K]^+$, calculated value), lariciresinol (10) (m/z 399.1210 $[M + K]^+$, calculated value), secoisolariciresinol (11)

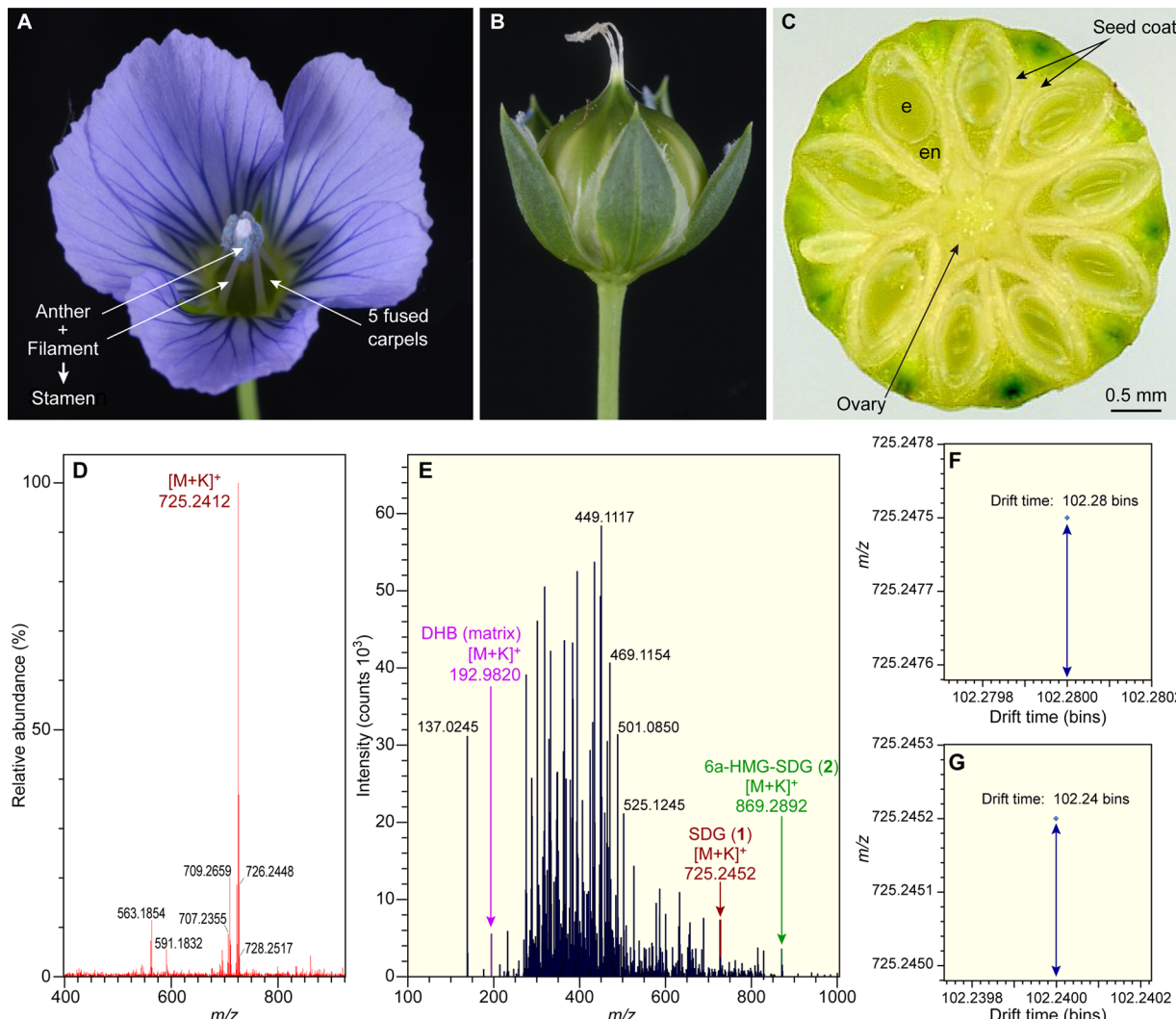


Figure 3. (A) Flax flower. (B) Flax capsule. (C) Cross-section of flax capsule at 7 DAF showing embryo (e), endosperm (en), seed coat, and ovary. (D) Positive ion mass spectrum of SDG (1) standard showing $[M + K]^+$. (E) Positive ion mass spectrum of flax capsule (6 DAF) cross-section depicting SDG (1) (red) and 6a-HMG SDG (2) (green). The MALDI MSI spectrum was acquired directly on a thin cross-section ($20 \mu\text{m}$ thickness) of a flax pod using 2,5-dihydroxybenzoic acid (DHB) as matrix. Under the conditions employed, the SDG (1) in the tissue was detected at nanomolar concentration relative to a known concentration of a SDG (1) standard. (F) Ion mobility mass spectrum of standard SDG (1) with drift time at 102.28 bins (5.4754 ms). (G) Ion mobility mass spectrum of SDG (1) in flax capsule (6 DAF) showing drift time at 102.24 bins (5.4732 ms).

(m/z 401.1366 $[M + K]^+$, calculated value), and 6a, 6a'-HMG SDG (3) (m/z 1013.3268 $[M + K]^+$ calculated value) were not detected under the conditions employed.

After the MALDI MSI experiment, capsule cross-sections were stained with toluidine blue O for anatomical visualization of embryo, endosperm, seed coat, and ovary tissue (Figures 4A,E). The MALDI MS images next established SDG (1, Figures 4B,F) and 6a-HMG SDG (2, Figure 4C, Figure S2A in the Supporting Information) were colocalized in developing seed coats at 6 and 7 DAF (Figure 4D, Figure S2B in the Supporting Information). Seeds that did not develop and those which were aborted (see * in Figures 4A,E) had no detectable ion signals for SDG (1) or 6a-HMG SDG (2) (Figures 4B,F).

We next sought to topographically profile relative SDG (1) levels using OpenMSI analysis capabilities;²⁰ this facile web-based interactive approach allows for localization of any selected specific mass in real time. Here, analysis of different regions in the seed coat (Figure 5, crosshairs) within a selected seed in the 7 DAF capsule (Figure 4F, yellow rectangle)

indicated that the SDG (1) ion was detectable at higher relative intensity levels in the area where the seed is attached to the ovary tissue (Figures 5A–D), with its overall relative intensity levels apparently gradually decreasing toward distal regions (Figures 5E–J).

Taken together, our MALDI MSI analyses indicated that SDG (1) and SDG-HMG (2) are mainly detectable at a relatively early development stage (6 and 7 DAF). These analyses though also provided some novel insights into the varying distribution of SDG (1) in the seed coat region at this early seed maturation stage (6 and 7 DAF). That is, SDG (1) was found to be nonuniformly distributed, being apparently most abundant toward the center of the capsule where the seed is attached to the ovary, and then progressively gradually decreasing in relative levels toward the outside. This may not be unexpected, as the region of seed attachment has vascular bundles that transports nutrients (and SDG (1) precursors) from the placenta to the developing embryo.^{28,29} These data thus seem to suggest that the lower detectability of SDG (1) in

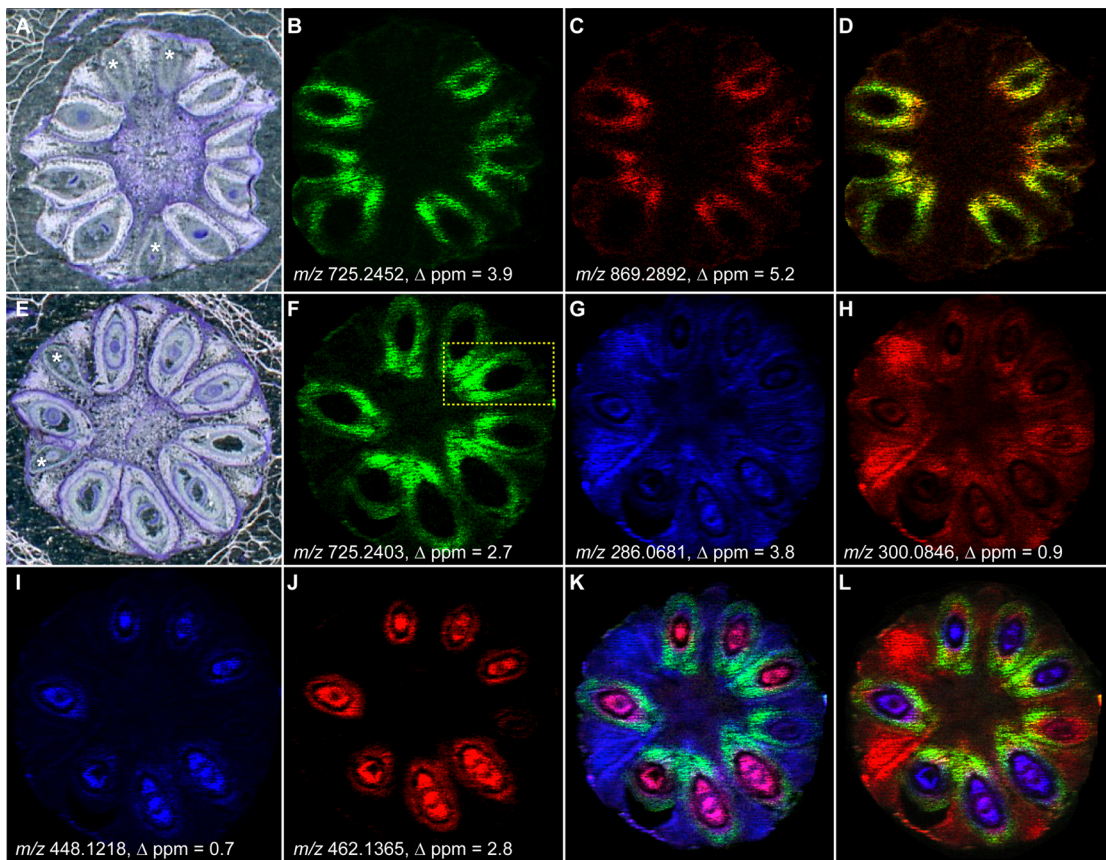


Figure 4. MALDI MS images of flax capsules. (A) Optical image of capsule (6 DAF) cross-section stained with toluidine blue O. (B, C) Positive ion $[M + K]^+$ MALDI MSI of 6 DAF flax capsule showing SDG (1, B, green) and 6a-HMG SDG (2, C, red). (D) Merged MALDI MSI of SDG (1) (green) and 6a-HMG SDG (2) (red) in 6 DAF capsule. (E) Optical image of capsule (7 DAF) cross-section stained with toluidine blue O. (F) Positive ion $[M + K]^+$ MALDI MSI of 7 DAF flax capsule showing SDG (1, green). (G-J) Positive ion $[M + K]^+$ MALDI MSI of 7 DAF flax capsule showing linamarin (4, G, blue), iotaustralin (5, H, red), linustatin (6, I, blue), and neolinustatin (7, J, red). (K) Merged MALDI MSI of SDG (1, green), linamarin (4, blue), and linustatin (6, red) in 7 DAF capsule. (L) Merged MALDI MSI of SDG (1, green), iotaustralin (5, red), and neolinustatin (7, blue) in 7 DAF capsule. All MALDI MS images were obtained at 20 μm spatial resolution. Scale: 5 mm. * in panels A and E indicates seeds that did not develop.

the more distal regions is due to its further conversion into the higher molecular weight phenolics. Interestingly, a previous study had localized SDG (1) epitopes to the seed coat sclerite secondary cell wall layers,^{27,30} although the chemical identity of what was actually detected was not established. Sclerite cell walls are also considered to provide the “hard body” of seed coats, and they are often described as being lignified.

Interestingly, however, neither SDG (1) nor SDG-HMG (2) was detected at earlier stages of flax capsule development or in the fully developed maturing seed of 10 and 12 DAF capsules. Moreover, in the 6 and 7 DAF capsule tissues, their precursors pinoresinol (9), lariciresinol (10), and secoisolariciresinol (11) were also not detected under the conditions employed. These findings are thus in general agreement with previous reports indicating that SDG (1) intermediate metabolites were undetectable at different stages of flax seed development using the methodologies then employed.^{2,31} This may imply rapid conversion of metabolites 9, 10, and 11 into SDG (1), SDG-HMG derivative 2, and higher molecular weight SDG-HMG derived phenolics. Furthermore, while we did not detect the 6a, 6a'-HMG SDG (3) lignan moiety in the flax capsule samples examined under the conditions employed, the ion intensity above m/z 900 was also very low. Consequently, the

mass accuracy obtained was insufficient for reliable annotation of this analyte 3.

It should be emphasized, however, that the additional OpenMSI capabilities also further enhanced our imaging capabilities by providing a web-based interactive resource, whereby localization of any detectable specific mass can be instantly established. This, in turn, allowed for metabolomics analyses via imaging vast numbers of metabolites in an interactive and comparative manner, thereby providing insights into metabolic processes never before achievable.

Gene Expression Profiles and Transcriptome Analysis of *LuDIR* and *LuPLR* Homologues. Whole capsules at 0, 3, 6, 12, 18, and 24 DAF and seeds at 3, 6, 12, 18, and 33 DAF were harvested to examine gene expression levels of *LuDIRs* and their downstream *LuPLRs* by quantitative real-time PCR (see Table S2 in the Supporting Information for primer sequences). In addition, transcriptome analyses (<http://uic.edu/pharmacy/MedPiTranscriptome/>) were conducted to compare expression patterns of *LuDIR* and *LuPLR* genes at either different flaxseed development stages (3 and 6 DAF) or in 12 and 18 DAF seed coats.

Through a bioinformatics analysis of the flax genome, a total of four putative *PLR* genes were identified herein, namely *Lus10012145*, *Lus10010403*, *Lus10012143*, and *Lus10007599*

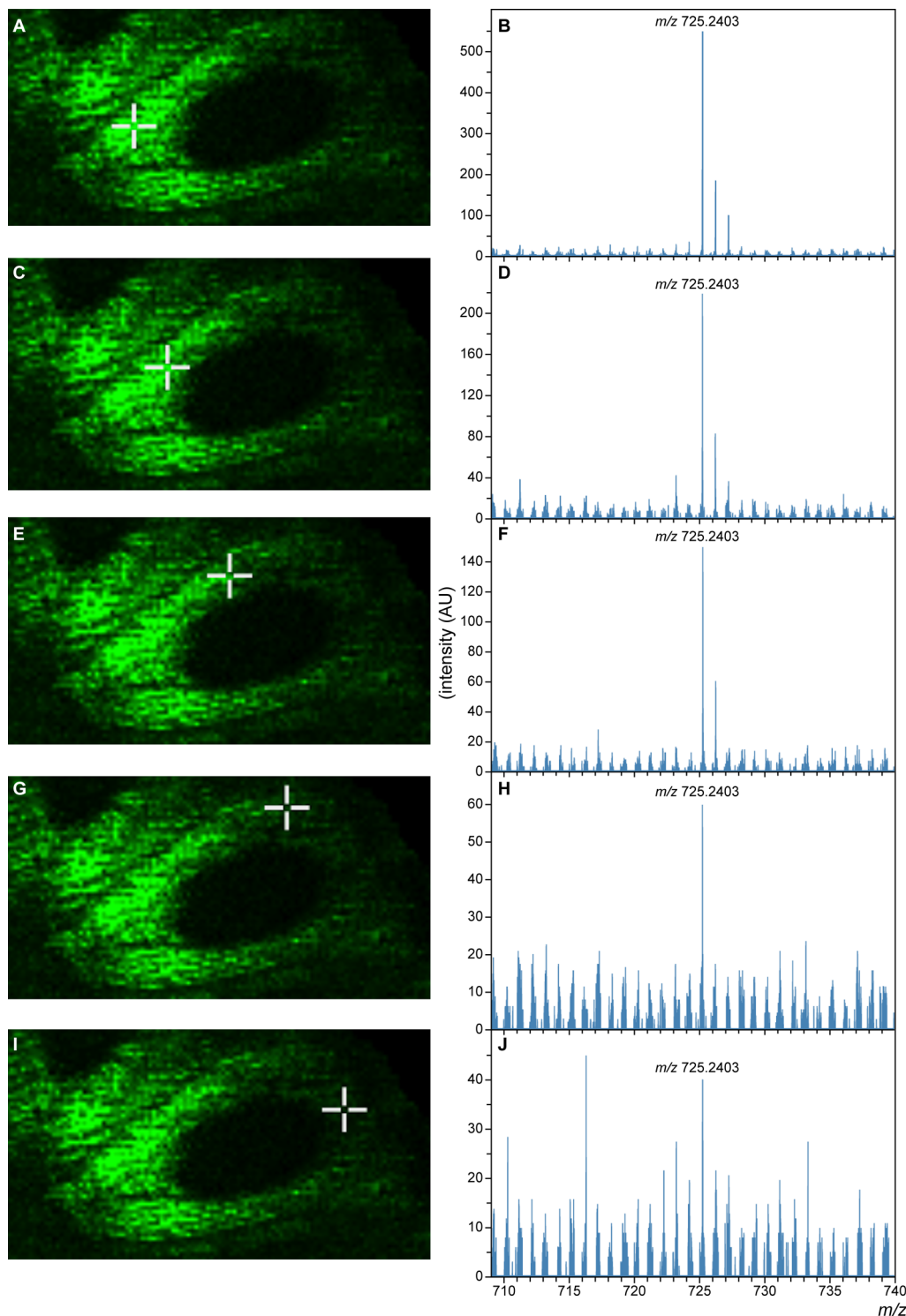


Figure 5. OpenMSI analysis highlighting relative spatiotemporal distributions of SDG (1). (A, C, E, G, and I) High-resolution MALDI MS images of flax seed at m/z 725.2403 [$M + K$]⁺ (see yellow dotted rectangle in Figure 4F) with cross-hairs to specify region of interest. (B, D, F, H, and J) Mass spectral intensities of m/z 725.2403 corresponding to cross-hairs in regions shown in A, C, E, G, and I, respectively.

(Figure S3 in the Supporting Information). Of these, two were previously functionally characterized as *bona fide* PLRs: LuPLR1 (identical a.a. sequence to Lus10012145) encodes a (−)-PLR which converts (−)-pinoresinol (**9b**) into (−)-lari- ciresinol (**10b**) and (+)-secoisolariciresinol (**11a**);¹³ LuPLR2 (95% a.a. identity to Lus10007599, with eight and six a.a. residues longer in the N- and C-terminal regions, respectively) encodes a (+)-PLR responsible for formation of (−)-secoiso-

lariciresinol (**11b**).³² The remaining two homologues, Lus10010403 and Lus10012143, show ~86% identity/∼ 93% similarity to LuPLR1, and are most likely (−)-PLRs, but they have not been characterized.

LuDIR5 and *LuDIR6*, encoding (−)-pinoresinol-forming DPs, were detected at highest levels in capsules at 0, 3, and 6 DAF (Figure 6A) and seeds at 3 and 6 DAF (Figure 6C), with expression levels gradually decreasing as capsule/seed develop-

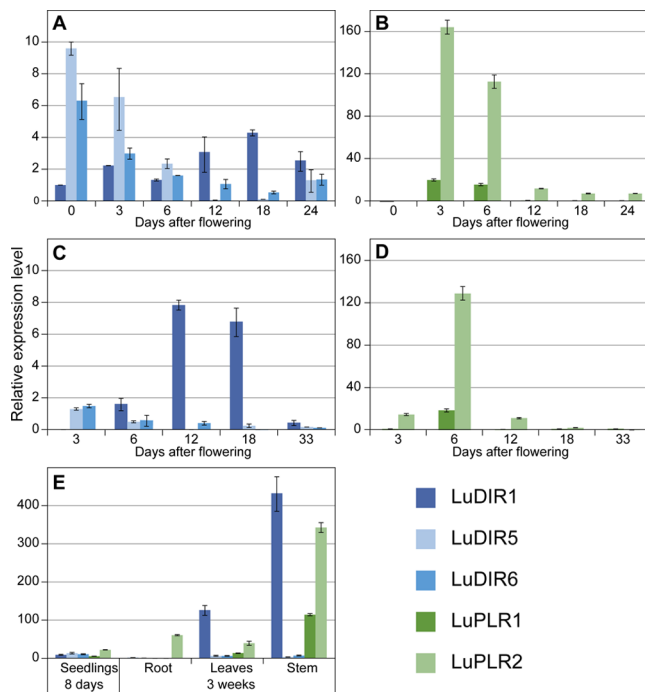


Figure 6. Expression profiles of DIR and PLR genes in *L. usitatissimum*. (A, B) *LuDIRs* (A) and *LuPLRs* (B) at different developmental stages of capsules. (C, D) *LuDIRs* (C) and *LuPLRs* (D) at different developmental stages of seeds. (E) *LuDIRs* and *LuPLRs* in 8-day-old seedlings, and 3 week-old stem, leaves and roots. Expression levels were normalized against the glyceraldehyde 3-phosphate dehydrogenase (GADPH) gene.⁴⁸

ment progressed. From the transcriptome analysis, *LuDIR6* transcripts were also detected at a very low level in 3 DAF whole seed (Figure S4A in the Supporting Information), whereas neither *LuDIR5* nor *LuDIR6* were detected in transcriptomes of seed coat tissues at later stages. Furthermore, expression of the *LuPLR1* gene above, encoding a (−)-PLR, was somewhat similar to *LuDIR5* or *LuDIR6* expression being expressed at 3–6 DAF in both flax capsule (Figure 6B) and seed tissues (Figure 6D). *LuPLR1* transcripts were, however, also observed in 6 DAF whole seed and in the 12 and 18 DAF seed coat in the transcriptome analysis (Figure S4B in the Supporting Information).

Moreover, the involvement of *LuPLR1* in SDG biosynthesis in flax seeds was further investigated using a loss of function strategy: RNAi-mediated *LuPLR1* gene silencing resulted in a 30–50-fold decrease in SDG (1) amounts, thus implicating *LuPLR1* in SDG (1) biosynthesis in flax seeds.³³

By contrast, expression of the *LuDIR1* gene, encoding a (+)-pinoresinol-forming DP, showed the reverse trend to *LuDIR5* and *LuDIR6*, gradually increasing in expression level up to 18 DAF in both whole capsules and seeds (Figures 6A,C). Expression of *LuPLR2*, encoding a (+)-PLR, was also highest in capsules at 3 and 6 DAF (Figure 6B) and seeds at 6 DAF (Figure 6D). Although not examined further, the other putatively annotated (+)-pinoresinol-forming DPs (*LuDIR2*, *LuDIR3*, and *LuDIR4*, Table 1) had the highest numbers of reads in 12 DAF seed coat tissues (Figure S4A in the Supporting Information). As regards the remaining two *PLRs*, *Lus10010403* also had highest read counts in 12 DAF flax seed coats, whereas *Lus10012143* was barely detected (Figure S4B in the Supporting Information).

Additionally, among other tissues (8 day-old seedlings and 3 week-old roots, stem, and leaves), *LuDIR1* showed predominant expression in 3-week-old leaves and stems (Figure 6E), whereas *LuDIR5* and *LuDIR6* were barely detectable.

Thus, in hindsight, our previous cloning attempts for a flax (−)-pinoresinol-forming DP had failed as our focus initially was primarily on seed coats collected at 12 and 18 DAF. That time frame was selected on the basis of results indicating that *LuPLR1*, encoding a (−)-PLR, was expressed in the seed coat.³¹ Following cloning and functional characterization of *LuDIRS* and *LuDIR6*, however, quantitative real-time PCR analyses indicated they were most highly expressed in capsules at 0 and 3 DAF (Figure 6A) and seeds at 3 DAF (Figure 6C), with expression levels rapidly declining as capsule and seed tissues developed—that is, thus presumably explaining our inability to clone a (−)-pinoresinol-forming DP from seed coats collected at the later time frames.

Recently, five *UDP-glycosyltransferase* (*UGT*) genes have also been reported from flax,³⁴ with only one (*UGT74S1*), coexpressed with *LuPLR1* at 8 and 16 DAF, found able to utilize secoisolariciresinol (11) as a substrate to form secoisolariciresinol monoglucoside and SDG (1), respectively when heterologously expressed in yeast. The stereospecificity of the glucosylation reaction was, however, not reported. Query of our transcriptome data also shows that *UGT74S1* has expression patterns similar to those of *LuPLR1* (Figure S4B in the Supporting Information), perhaps suggesting that these pathway genes are coexpressed.

These results thus demonstrate the presence of two temporally distinct pathways using first (−)-DPs (*LuDIRS*/*LuDIR6*) and then subsequently (+)-DPs (i.e., *LuDIR1*) in the developing flax seed tissues to ultimately afford (+)- and (−)-SDG (1a and 1b), respectively, in a ca. 99:1 product ratio. This, in turn, suggests potential, but yet unknown, differences in the biological/biochemical function of these two diastereomeric forms of SDG (1) in the seed coat tissues. On the other hand, *LuDIR1* expression in leaves and stems is in agreement with the presence of (+)-pinoresinol (9a) derived lignans in these tissues.¹⁴

The patterns of gene expression and differential SDG (1) distribution thus also raises the question of the role(s) of the different cells that are involved in the biosynthesis and transport of SDG (1) and/or its derivatives.

Comparative Spatiotemporal Mapping of Cyanogenic Glucosides in Developing Flax Capsule by MALDI MSI. Although previous studies reported accumulation of cyanogenic glucosides in flax stem, root, flower, and seed tissues,^{23,35} their spatiotemporal distributions *in situ* have not been reported until now. It was next considered instructive to ascertain where and when plant defense cyanogenic glucosides accumulated in developing capsule tissues.^{21–23} Here, however, our high spatial resolution MALDI MSI results indicated that cyanogenic monoglucosides 4 and 5 were detected throughout the flax capsules from 0 DAF until 7 DAF, including the ovary, seed coat, and embryo tissues (Figures 4G,H and Figure 3C for flax capsule anatomy), but not at later stages (10 and 12 DAF). More specifically, in the 7 DAF capsule, potassium adducts of the monoglucosides linamarin (4) *m/z* 286.0681 (Δ ppm 4.2) and lotaustralin (5) 300.0846 (Δ ppm 0.9) were observed (Figure S1 in the Supporting Information). Laminarin (4) identity was further confirmed by IMS, as drift times of both authentic linamarin (4) and linamarin (4) in flax tissues were 48.00 (2.5666 ms) and 48.06 bins (2.5698 ms), respectively

(Figure S5 in the Supporting Information). We further deduced the identity of linamarin (**4**) by the isotopic peak ratios (Figure S6 in the Supporting Information) and CID MS/MS fragmentation of the authentic standard and flax seed compound (i.e., 286 [M + K]⁺ and 271 [M + K - CH₃]⁺). Additionally, the identity of lotaustralin (**5**) was apparently confirmed by CID MS/MS fragmentation of its [M + K]⁺ ion at *m/z* 300.06, through detection of three major fragments at 25 eV, namely, loss of water at *m/z* 282, the aglycone at *m/z* 137 (the most abundant peak corresponding to product ion from Y₀⁺ cleavage^{36,37}) and a C₁⁺ fragmentation ion at *m/z* 218 (monosaccharide residue).

Potassium adducts of the diglucosides, linustatin (**6**) and neolinustatin (**7**), were also readily identified at *m/z* 448.1218 (Δ ppm 0.7) and 462.1365 (Δ ppm 2.8) (Figure S1 in the Supporting Information), respectively, with identities further verified by CID MS/MS analyses, that is, fragmentation patterns of **6** at 30 eV collision energy gave characteristic terminal glucoside fragmentation motifs,³⁶⁻³⁸ with fragment ions at *m/z* 365, 339, 329, 325, and 299, respectively, as shown (Figure S7 in the Supporting Information). Similarly, the CID MS/MS fragmentation pattern of neolinustatin (**7**) (acquired at 40 eV) also had analogous sugar ring fragmentation pattern at *m/z* 379, 353, 343, 339, and 313 (Figure S8 in the Supporting Information). A sixth ion observed at *m/z* 283 results from loss of glucose.^{36,37}

To establish cyanogenic glucoside spatiotemporal distribution, we next studied flax capsules at different developmental stages (0, 3, 4, 6, 7, 10, and 12 DAF) as before. The cyanogenic monoglucosides **4** and **5** were detected in young flax capsules (0, 3, 4, 6, and 7 DAF, Table S3 in Supporting Information) with linamarin (**4**), based on relative signal intensity counts, being higher in relative amount as compared to **5** at 0, 3, and 4 DAF. More specifically, the potassium adducts corresponding to **4** and **5** were observed throughout the tissues of the 7 DAF flax capsule (Figures 4G,H and Figure 3C for flax anatomy). Although these ions were found at 0, 3, 4, and 6 DAF, the ions were also dispersed throughout the capsule and no distinctive spatial distribution were readily observed. Neither **4** nor **5** were detected at 10 and 12 DAF.

In contrast, cyanogenic diglucoside MALDI MS images were quite distinct. Linustatin (**6**) and neolinustatin (**7**) were specifically localized to the flax seed embryo and endosperm (Figures 4I,J), but they were not detected in the seed coat and ovary; additionally, cyanogenic diglucoside **6** was detected in all developmental stages examined (Table S3 in Supporting Information), with an initial low ion abundance (1245 intensity counts) at 0 DAF and increasing relative ion intensity as the capsule progressed to maturity (i.e. a ca. 15-fold increase in signal intensity counts at 12 DAF occurred). Neolinustatin (**7**) though was only detected in more mature flax tissues (7, 10, and 12 DAF). As for SDG (**1**) and SDG-HMG (**2**), aborted and empty seeds did not show ions for linustatin (**6**) and neolinustatin (**7**). In sum, despite the potential vulnerability of cyanogenic glucosides to rapid β-glucosidase catalyzed degradation upon cellular disruption,^{39,40} which could possibly occur during tissue cryosectioning, our MALDI MSI protocol nevertheless allowed their detection.

It was also known from earlier work, however, that cyanogenic monoglucosides **4** and **5** undergo further glucosylation to form **6** and **7** as the capsules progress to maturity,³⁹ with the diglucosides herein found to be spatially distributed specifically in flax seed endosperm and embryo

tissues by 6–7 DAF (Figures 4I,J). These MALDI imaging findings are thus in agreement with previous reports that cyanogenic glucoside contents in flax tissues vary with age and developmental stage,^{22,23,35,41} with the mature embryo specifically being where cyanogenic diglucosides storage occurs.

While the presumed translocation mechanism of these cyanogenic compounds into the seed is not known, it has been proposed that cyanogenic monoglucosides are transported there in modified form (e.g., as diglucosides **6** and **7**) for protection against β-glucosidase cleavage of the monoglucosides to liberate HCN.^{39,40} These diglucosides are then considered to be stored as such in unaltered form until the seed enters the germination phase, where they are reportedly hydrolyzed back to monoglucosides or completely hydrolyzed without accumulation of monoglucosides forming acetone cyanohydrin, which dissociates into acetone and HCN.^{22,35,39} Subsequently, the HCN is recycled to asparagine by β-cyanoalanine synthase.^{39,42} This storage mechanism thus suggests a potential role of cyanogenic compounds as N-storage compounds that could be later used for amino acid synthesis during germination.³⁹

The biosynthetic pathway to linamarin (**4**) and lotaustralin (**5**) has been elucidated in cassava (*Manihot esculenta*). First, L-valine and L-isoleucine are converted into their corresponding oximes by two cytochrome P-450s, CYP79D1 and CYP79D2 which are 85% identical to each other,⁴³ catalyzing conversion of both Ile and Val into the corresponding oximes. The next step involving formation of the corresponding cyanohydrins is also catalyzed by a bifunctional cytochrome P-450, CYP71E7.⁴⁴ In the last step, the unstable cyanohydrins are glucosylated by two UDP glucosyltransferase, UGT85K4 and UGT85K5 (96% identical to each other).⁴⁵ All of these have been shown to be expressed in the same tissue in cassava.⁴⁵

Query of the flax genome identified six CYP79D1 homologues (~59–63% identity), two CYP71E7 homologues (52–59%), and 12 UDP glucosyltransferases (~45–55% identity to UGT85K4), as possible candidates in the biosynthetic pathway to linamarin (**4**) and lotaustralin (**5**) in flax. One CYP79D1 homologue (Lus10023144) and the two CYP71E7 homologues (Lus10023140 and Lus10011499) were highly expressed in 3 and 6 DAF whole seeds (Figure S9A in the Supporting Information), with two UDP glucosyltransferases, Lus10013924 and Lus10000632, also present but at lower levels (Figure S9B in the Supporting Information). Interestingly, this is where both linamarin (**4**) and lotaustralin (**5**) were localized at 0, 3, 4, 6, and 7 DAF, and thus, they can provisionally be considered as being involved in their biosynthesis.

Using a combination of integrated transcriptomics and bioinformatics approaches, it was possible to further deduce the genes encoding the DP and PLR proteins responsible for stereoselective coupling and downstream enantiomeric pathway steps to SDG (**1**), and to gain new insights into their further conversions of the products formed into higher molecular weight phenolics accumulating in the maturing seed coats. Moreover, our high-resolution MALDI MSI analyses permitted determination of the spatiotemporal distribution and localization of the oligomeric lignan intermediates, as well as the cyanogenic glucosides in flax, thereby providing novel insights on the complexity of their metabolite distribution/accumulation in living cells. Our work thus demonstrates the spatiotemporal localization of SDG (**1**) directly from a single cross-section of flax capsule tissue and without recourse of

tedious extraction and purification methodologies. Furthermore, it also provides direct evidence that spatiotemporal distribution/accumulation of the oligomeric lignans and cyanogenic glucosides are both chemotype- and cell type/tissue-specific; that is, oligomeric lignans are distributed in the seed integument/seed coat, while cyanogenic glucosides are in the ovary, endosperm and embryo (Figures 4K,L). Taken together, these integrated omics approaches provide new insights into the complexities of seed development processes in economically important plants such as flax.

■ EXPERIMENTAL SECTION

General Experimental Procedures. Flax (*Linum usitatissimum*, L.) seeds were from Horizon Herbs, LLC (Williams, OR, U.S.A.), with plants maintained at the Washington State University greenhouse facilities under a daily cycle of 16 h of light (23 °C) and 8 h of dark (19 °C). Flowers were individually tagged when fully opened (anthesis), with that time point called zero day after flowering (DAF), with capsules harvested as needed.

Isolation of LuDIR Homologues. Cloning of the *LuDIR1* gene was conducted using PCR-based genome walking. First, genomic DNA was isolated from flax seed using CTAB buffer. The nested consensus region was amplified with PS_6forward and PS_2reverse degenerate primers (Table S1 in the Supporting Information), with upstream and downstream regions obtained according to the GenomeWalker (Clonetech, Mountain View, CA) procedure using primary and nested gene specific primers.¹⁶ To ensure the gene was actively transcribed in flax seed, both gene-specific (Flax_1GSP) and 5'-race primers were used to amplify transcript from flax seed.

LuDIR5 and *LuDIR6* genes were obtained from genomic DNA extracted from 2 week-old whole flax seedlings using a DNeasy Plant Mini kit (Qiagen) according to the manufacturer's instructions. Individual genes were amplified using PCR with each gene specific primer (Table S1). Amplified products were individually subcloned into pCR4-TOPO vector and sequences were verified.

Heterologous Expression and Purification of LuDIR1 in Insect Cell Cultures. To express recombinant *LuDIR1* in insect (*Drosophila melanogaster* Schneider2) cells, the *LuDIR1* gene was amplified from the *LuDIR1*/pCR2.1–TOPO vector (Invitrogen) with M13 forward and reverse primers. The amplified 564-bp *LuDIR1* gene was subcloned into the pMT/V5-TOPO vector (Invitrogen). After sequence verification, the *LuDIR1*/pMT/V5-TOPO vector was cotransfected with the pCoHygro vector using $\text{Ca}_3(\text{PO}_4)_2$. Transfected cells were screened using hygromycin ($300 \mu\text{g mL}^{-1}$) containing HyQ-SFX insect cell medium (HyClone). Cell cultures were gradually scaled up from 5 mL to 2 L, and cells were induced with $900 \mu\text{M CuSO}_4$ for 40 h at 26 °C. Cells (3 L) were harvested by centrifugation (1000g, 15 min and 12 000g, 30 min) with supernatants concentrated (Amicon concentrator, Model 2000) under nitrogen gas pressure using a PM-10 membrane (Amicon) to less than 200 mL. The concentrate was next fractionated with $(\text{NH}_4)_2\text{SO}_4$, with protein precipitating between 40 and 80% saturation further purified with a series of cationic column chromatographic steps [SP-Sepharose Fast Flow (GE Healthcare), Mono S 5/50 (GE Healthcare), and POROS 20 SP (Applied Biosystems) columns, successively]. Detailed procedures are as described in Kim et al.⁶

Heterologous Expression and Purification of LuDIR5 and LuDIR6 in Tomato Cell Suspension Cultures. Both

LuDir5 and *LuDIR6* genes were reamplified with Kozak sequence⁴⁶ and *Hind*III restriction site containing primers (Table S1 in the Supporting Information) and then individually cloned into the pCR4-TOPO vector. After sequence verification, both genes were individually excised with restriction enzyme (*Eco*RI and *Hind*III) and ligated in the same site of the pART17 vector.⁶

Each individual *LuDIR*/pART17 plasmid was coated on gold particles for biolistic bombardment of tomato (*Solanum peruvianum*) cell suspension cultures, with transformation and transformed calli screening conducted following procedures by Kim et al.⁶ After screening kanamycin-resistant transgenic calli, gene expression levels in individual tomato calli were assessed by RT-PCR. Three calli lines with the highest mRNA expression levels were chosen for subsequent suspension cell culture work. Suspension cell cultures were scaled-up gradually by inoculating into new medium every week. Seven days after final inoculation in 3 L of medium, plant cells were harvested by vacuum filtration with cell wall-bound proteins recovered by filtration after agitating cells in 0.1 M K_3PO_4 (pH 5.9) containing 75 mM and 150 mM KCl, respectively. Both fractions were mixed with a SP-Sepharose Fast Flow resin (80 mL), and equilibrated with 75 mM KCl in 0.1 M K_3PO_4 . Proteins were eluted with 1 M NaCl in K_3PO_4 buffer and fractionated with $(\text{NH}_4)_2\text{SO}_4$. Recombinant proteins were purified as for *LuDIR1*, with protein purity examined using SDS-PAGE and protein identity confirmed by peptide sequencing.

Dirigent Protein Assays. Recombinant DPs were assayed with *Trametes versicolor* laccase as oxidizing agent and coniferyl alcohol (8) in 40 mM MES buffer to a total volume of 250 μL . After incubation for 4 h in a 30 °C shaking incubator, each assay mixture was extracted twice with 500 μL of EtOAc, dried *in vacuo*, redissolved in MeOH–H₂O (3:7, v/v), and subjected to reversed-phase HPLC.⁶ Fractions containing enzymatically formed pinoresinol (9) were collected, freeze-dried, and subjected to chiral HPLC analysis.⁴⁷ The latter used a Daicel Chiralcel OD column (250 × 4.6 mm, Chiral Technologies, Inc., West Chester, PA) eluted with EtOH–hexanes (1:1), at a flow rate of 0.8 mL min⁻¹.

Quantitative Real Time PCR. Total RNA was individually isolated from whole capsules (6–10) at 0, 3, 6, 12, 18, and 24 DAF, whole seeds (10–30) at 3, 6, 12, 18, and 33 DAF, 8 day-old seedlings (20), as well as stem, leaves, and roots from 3 week-old plants (3). Each sample was individually flash frozen in liquid nitrogen and stored at –80 °C until needed. Each frozen plant sample was ground in a mortar by means of a pestle, transferred into 2 mL microcentrifuge tubes containing a stainless steel bead (5 mm mean diameter), and pulverized using a TissueLyserII (Qiagen). RNA was initially isolated using PureLink Plant RNA reagent (Invitrogen) and then further purified using the Spectrum Total RNA kit (Sigma). First-strand cDNA was then synthesized using the PrimeScript first strand cDNA Synthesis kit (Takara) after DNaseI treatment (Invitrogen). Gene amplification was performed using Platinum SYBR Green qPCR SuperMix-UDG (Invitrogen) for quantitative real-time PCR. Reaction mixtures included synthesized first-strand cDNA, forward and reverse gene specific primers (Table S2 in the Supporting Information), which were designed using the Primer Premier Software (Biosoft International), SYBR Green qPCR SuperMix, and ROX Reference Dye. A Stratagene Mx3005p QPCR System was used for real-time qPCR gene amplification. Expression

levels were normalized against the glyceraldehyde 3-phosphate dehydrogenase (GADPH) gene,⁴⁸ with expression levels for either the *LuDIR1* or *LuPLR1* genes in 0 DAF capsules set to 1.

Flax Seed Transcriptome Analysis Preparation. Total RNA was extracted from whole seeds (collected 3 and 6 DAF) or seed coats (harvested 12 and 18 DAF) using a modification of the method by Verwoerd et al.,⁴⁹ involving addition of high molecular weight polyethylene glycol⁵⁰ as follows: Approximately 100 mg each of ground whole seeds or seed coats were individually placed into precooled 2 mL microcentrifuge tubes containing 1–2% (w/v) high molecular weight-polyethylene glycol (HMW-PEG 20,000, Fluka), these being mixed with 500 μ L hot (80 °C) extraction buffer consisting of a 1:1 mixture of phenol (pH 4.3 ± 0.2, Sigma) and total RNA extraction buffer [100 mM Tris-HCl (Sigma), 0.1 M LiCl (Sigma), 10 mM EDTA (Sigma), 1% SDS (pH 8.0)]. Each mixture was homogenized by vortexing for 30 s, with 250 μ L of a mixture of CHCl₃ and isoamyl alcohol (24:1) added, and the whole vortexed for 30 s. After centrifugation for 5 min at 18 000g at room temperature, each aqueous phase was carefully removed and placed into new 1.5 mL microcentrifuge tubes, these being individually mixed with equal volumes of 4 M LiCl. Total RNA samples were allowed to precipitate overnight and collected by centrifugation at 18 000g for 10 min at 4 °C. Each pellet was dissolved in 250 μ L of DEPC-treated H₂O, following which a one tenth volume of 3 M NaOAC (pH 5.2) was added; in each case, total RNA was precipitated with 2 volumes of EtOH. Each total RNA pellet was collected by centrifugation at 18 000g for 10 min at 4 °C, washed with 70% aqueous EtOH. Total RNA pellet samples were dried, dissolved in 50 μ L of DEPC-treated H₂O with 25 μ g of each samples used for transcriptome sequencing and library assembly as described in Marques et al.⁵¹ Final assembly for all tissues can be accessed at <http://uic.edu/pharmacy/MedPiTranscriptome/>

MALDI Imaging Mass Spectrometry. The matrix 2,5-dihydroxybenzoic acid (5 mg mL⁻¹ in MeOH) was used to test ionization of the SDG (**1**) standard. To map its localization in flax capsules, the MALDI MSI protocol developed for *Podophyllum* species plant tissue was followed.¹⁹ Fresh flax developing capsules (0, 3, 4, 6, 7, 10, and 12 DAF) were harvested from the greenhouse, with each embedded in agarose (3%), cryo-sectioned at 20 μ m thickness, after which matrix (DHB, 40 mg mL⁻¹) was applied by an automated sprayer (TM-Sprayer, HTX Technologies).

MALDI MSI was carried out using SYNAPT G2 High Definition Mass Spectrometry (HDMS) system with TriWave technology (Waters). Mass calibration was performed using red phosphorus cluster ions. MALDI-TOF data was acquired in the positive ion mode at a resolution range of *m/z* 100 to 1000 Da with spatial resolution of 100 and 20 μ m at laser energy setting of 350 and firing rate of 1000 Hz. The lock mass used in the experiment was leucine enkephalin, C₂₈H₃₇N₅O₇ with *m/z* 556.2771 [M + H]⁺. The area selected for imaging was defined using HDImaging software (V1.2, Waters). There were about 70 000 laser shots per tissue sample (area, 27.5 mm²) at a sampling rate of 0.5 s per pixel. Ion mobility data were acquired at the following settings: (a) TriWave DC: bias at 40.0, (b) TriWave IMS: wave velocity at 650 m s⁻¹ and wave height at 40 V, (c) TriWave transfer: wave velocity at 279 m s⁻¹ and wave height at 4 V, (d) IMS configuration: IMS wave velocity start velocity at 700 m s⁻¹ and end velocity at 270 m s⁻¹. Helium cell gas flow was at 180 and IMS gas flow was 90 mL⁻¹ min⁻¹. The raw data were then processed and ion maps were visualized in

HDImaging software (V1.2, Waters) to create ion-density maps, normalize peak intensity, adjust color scale, quantify ion intensity and drift time (bin) spectrum. The drift time in bins were converted into milliseconds using the equation:

$$DT_c = \frac{DT - (EDC_{\text{Offset}} \times (\sqrt{m/z}))}{1000}$$

where

DT_c = corrected Drift time

DT = measured time in bins *(total time in milliseconds/200 bins)

EDC_{offset} = Enhanced Duty Cycle (depending on instrument setting)

m/z = measured mass

Collision-induced dissociation and tandem mass spectrometry, CID MS/MS analysis was performed between 25 to 75 eV.

Furthermore, OpenMSI (<http://openmsi.nersc.gov>)²⁰ was employed to advance the visualization and analysis of the MALDI MSI data and to obtain accurate localization of analytes in flax tissues. The images associated with this study are publicly available for web-based visualization and download via the OpenMSI science gateway. To achieve this, data were transferred from Washington State University to the National Energy Research Scientific Computing Center (NERSC) using ESNet, with files loaded from the *.img file format into the OpenMSI fileformat.²⁰ Once converted, individual ions could be selected on the basis of precise specification of *m/z* bonds at submillidalton specification as shown. Red, green, and blue images correspond to three different ions overlaid (e.g., Figures 4K,L). Where pixels are predominantly “red”, the ion associated with the red channel is proportionally higher than the other two ions; where pixels are “green”, the ion associated with the green channel is proportionally higher, and so forth. Interesting comparisons could be stored as a persistent web-URL. These URLs were shared and enabled accelerated investigation of the vast amount of data generated by a MSI experiment.

Plant tissue samples were also stained with toluidine blue O after MALDI imaging analysis for histological profiling analysis directly on MALDI imaged tissues.¹⁹

ASSOCIATED CONTENT

Supporting Information

Primers used to isolate LuDP homologues and for quantitative RT-PCR analyses, amino acid sequence comparison, and temporal expression of pathway genes, as well as MALDI MSI, IMS, and CID MS/MS data for compounds **1**, **2**, **4**, **5**, **6**, and **7**. The Supporting Information is available free of charge on the ACS Publications website at DOI: 10.1021/acs.jnatprod.5b00023.

AUTHOR INFORMATION

Corresponding Author

*E-mail lewison@wsu.edu. Tel. 1 509 335 2682. Fax: 1 509 335 8206.

Notes

The authors declare no competing financial interest.

ACKNOWLEDGMENTS

The Chemical Sciences, Geosciences and Biosciences Division, DOE Office of Basic Energy Sciences (DE-FG-0397ER20259)

is thanked for providing the primary support for the MALDI mass spectrometry imaging and recombinant dirigent protein experimental work/analyses. Thanks are also extended to the National Science Foundation (MCB-1052557), and the G. Thomas and Anita Hargrove Center for Plant Genomic Research, for additional generous financial support. MALDI-MS based imaging analysis was performed on an instrument acquired through a Major Research Instrumentation grant (DBI-1229749) from the National Science Foundation. B.P.B. and O.R. lead the OpenMSI project hosted at the National Energy Research Scientific Computing Center (NERSC) which is supported by the Office of Science of the U. S. Department of Energy under contract DE-AC02-05CH11231. We thank Mark Towers, Emmanuelle Claude, and Tasneem Bahrainwala of Waters Corporation for instrumentation technical assistance. Thanks are also extended to Mia Ryckman for technical assistance.

■ REFERENCES

- (1) Struijs, K.; Vincken, J.-P.; Doeswijk, T. G.; Voragen, A. G. J.; Gruppen, H. *Phytochemistry* **2009**, *70*, 262–269.
- (2) Ford, J. D.; Huang, K.-S.; Wang, H.-B.; Davin, L. B.; Lewis, N. G. *J. Nat. Prod.* **2001**, *64*, 1388–1397.
- (3) Kamal-Eldin, A.; Peerlkamp, N.; Johnsson, P.; Andersson, R.; Andersson, R. E.; Lundgren, L. N.; Åman, P. *Phytochemistry* **2001**, *58*, 587–590.
- (4) Westcott, N. D.; Muir, A. D. *Phytochem. Rev.* **2003**, *2*, 401–417.
- (5) Davin, L. B.; Wang, H.-W.; Crowell, A. L.; Bedgar, D. L.; Martin, D. M.; Sarkanen, S.; Lewis, N. G. *Science* **1997**, *275*, 362–366.
- (6) Kim, K.-W.; Moinuddin, S. G. A.; Atwell, K. M.; Costa, M. A.; Davin, L. B.; Lewis, N. G. *J. Biol. Chem.* **2012**, *287*, 33957–33972.
- (7) Pickel, B.; Constantin, M.-A.; Pfannstiel, J.; Conrad, J.; Beifuss, U.; Schaller, A. *Angew. Chem., Int. Ed.* **2010**, *49*, 202–204.
- (8) Vassão, D. G.; Kim, K.-W.; Davin, L. B.; Lewis, N. G. In *Comprehensive Natural Products Chemistry II*, Mander, L. N., Liu, H.-W., Eds. Elsevier: Oxford, U.K., 2010; Vol. 1, pp 815–928.
- (9) Kim, K.-W.; Smith, C. A.; Daily, M. D.; Cort, J. R.; Davin, L. B.; Lewis, N. G. *J. Biol. Chem.* **2015**, *290*, 1308–1318.
- (10) Seneviratne, H. K.; Dalisay, D. S.; Kim, K.-W.; Moinuddin, S. G. A.; Yang, H.; Hartshorn, C. M.; Davin, L. B.; Lewis, N. G. *Phytochemistry* **2015**, DOI: 10.1016/j.phytochem.2014.10.013.
- (11) Nakatsubo, T.; Mizutani, M.; Suzuki, S.; Hattori, T.; Umezawa, T. *J. Biol. Chem.* **2008**, *283*, 15550–15557.
- (12) Dinkova-Kostova, A. T.; Gang, D. R.; Davin, L. B.; Bedgar, D. L.; Chu, A.; Lewis, N. G. *J. Biol. Chem.* **1996**, *271*, 29473–29482.
- (13) Von Heimendahl, C. B. I.; Schäfer, K. M.; Eklund, P.; Sjöholm, R.; Schmidt, T. J.; Fuss, E. *Phytochemistry* **2005**, *66*, 1254–1263.
- (14) Schmidt, T. J.; Hemmati, S.; Fuss, E.; Alfermann, A. W. *Phytochem. Anal.* **2006**, *17*, 299–311.
- (15) Fujita, M.; Gang, D. R.; Davin, L. B.; Lewis, N. G. *J. Biol. Chem.* **1999**, *274*, 618–627.
- (16) Ford, J. D. Ph.D. Thesis, Washington State University, 2001; p 246.
- (17) Teoh, K. H.; Ford, J. D.; Kim, M.-R.; Davin, L. B.; Lewis, N. G. In *Flaxseed in Human Nutrition*, 2nd ed.; Thompson, L. U.; Cunnane, S. C., Eds. AOCS Press: Champaign, IL, 2003; pp 41–62.
- (18) Costa, M. A.; Marques, J. V.; Dalisay, D. S.; Herman, B.; Bedgar, D. L.; Davin, L. B.; Lewis, N. G. *PloS One* **2013**, *8* (12), e83169.
- (19) Marques, J. V.; Dalisay, D. S.; Yang, H.; Lee, C.; Davin, L. B.; Lewis, N. G. *Mol. BioSyst.* **2014**, *10*, 2838–2849.
- (20) Rübel, O.; Greiner, A.; Cholia, S.; Louie, K.; Bethel, E. W.; Northen, T. R.; Bowen, B. P. *Anal. Chem.* **2013**, *85*, 10354–10361.
- (21) Kakes, P. *Euphytica* **1990**, *48*, 25–43.
- (22) Krech, M. J.; Fieldes, M. A. *Can. J. Bot.* **2003**, *81*, 1029–1038.
- (23) Niedzwiedź-Siegięń, I. *Phytochemistry* **1998**, *49*, 59–63.
- (24) Kim, M. K.; Jeon, J.-H.; Fujita, M.; Davin, L. B.; Lewis, N. G. *Plant Mol. Biol.* **2002**, *49*, 199–214.
- (25) Wang, Z.; Hobson, N.; Galindo, L.; Zhu, S.; Shi, D.; McDill, J.; Yang, L.; Hawkins, S.; Neutelings, G.; Datla, R.; Lambert, G.; Galbraith, D. W.; Grassa, C. J.; Gerald, A.; Cronk, Q. C.; Cullis, C.; Dash, P. K.; Kumar, P. A.; Cloutier, S.; Sharpe, A. G.; Wong, G. K.-S.; Wang, J.; Deyholos, M. K. *Plant J.* **2012**, *72*, 461–473.
- (26) Atwell, K. M. Master's Thesis, Washington State University, 2001, 121.
- (27) Attoumbré, J.; Mahamane Laoualy, A. B.; Bienaimé, C.; Dubois, F.; Baltora-Rosset, S. *Phytochem. Lett.* **2011**, *4*, 194–198.
- (28) Moïse, J. A.; Han, S.; Gudynaitė-Savitch, L.; Johnson, D. A.; Miki, B. L. A. *In Vitro Cell. Dev. Biol. Plant* **2005**, *41*, 620–644.
- (29) Wang, H. L.; Grusak, M. A. *Ann. Bot.* **2005**, *95*, 737–747.
- (30) Attoumbré, J.; Bienaimé, C.; Dubois, F.; Fliniaux, M.-A.; Chabbert, B.; Baltora-Rosset, S. *Phytochemistry* **2010**, *71*, 1979–1987.
- (31) Hano, C.; Martin, I.; Fliniaux, O.; Legrand, B.; Gutierrez, L.; Arroo, R. R. J.; Mesnard, F.; Lamblin, F.; Lainé, E. *Planta* **2006**, *224*, 1291–1301.
- (32) Hemmati, S.; von Heimendahl, C. B. I.; Klaes, M.; Alfermann, A. W.; Schmidt, T. J.; Fuss, E. *Planta Med.* **2010**, *76*, 928–934.
- (33) Renouard, S.; Tribalatc, M.-A.; Lamblin, F.; Mongelard, G.; Fliniaux, O.; Corbin, C.; Marosevic, D.; Pilard, S.; Demaily, H.; Gutierrez, L.; Hano, C.; Mesnard, F.; Lainé, E. *J. Plant Physiol.* **2014**, *171*, 1372–1377.
- (34) Ghose, K.; Selvaraj, K.; McCallum, J.; Kirby, C. W.; Sweeney-Nixon, M.; Cloutier, S. J.; Deyholos, M.; Datla, R.; Fofana, B. *BMC Plant Biol.* **2014**, *14*, 82.
- (35) Frehner, M.; Scalet, M.; Conn, E. E. *Plant Physiol.* **1990**, *94*, 28–34.
- (36) Domon, B.; Costello, C. *Glycoconjugate J.* **1988**, *5*, 397–409.
- (37) Ma, Y. L.; Li, Q. M.; Van den Heuvel, H.; Claeys, M. *Rapid Commun. Mass Spectrom.* **1997**, *11*, 1357–1364.
- (38) Vukics, V.; Guttman, A. *Mass Spectrom. Rev.* **2010**, *29*, 1–16.
- (39) Selmar, D.; Lieberei, R.; Biehl, B. *Plant Physiol.* **1988**, *86*, 711–716.
- (40) Gruhnert, C.; Biehl, B.; Selmar, D. *Planta* **1994**, *195*, 36–42.
- (41) Fan, T. W.-M.; Conn, E. E. *Arch. Biochem. Biophys.* **1985**, *243*, 361–373.
- (42) Miller, J. M.; Conn, E. E. *Plant Physiol.* **1980**, *65*, 1199–1202.
- (43) Andersen, M. D.; Busk, P. K.; Svendsen, I.; Möller, B. L. *J. Biol. Chem.* **2000**, *275*, 1966–1975.
- (44) Jørgensen, K.; Vinther Morant, A. V.; Morant, M.; Jensen, N. B.; Olsen, C. E.; Kannangara, R.; Motawia, M. S.; Möller, B. L.; Bak, S. *Plant Physiol.* **2011**, *155*, 282–292.
- (45) Kannangara, R.; Motawia, M. S.; Hansen, N. K. K.; Paquette, S. M.; Olsen, C. E.; Möller, B. L.; Jørgensen, K. *Plant J.* **2011**, *68*, 287–301.
- (46) Nakagawa, S.; Niimura, Y.; Gojobori, T.; Tanaka, H.; Miura, K.-i. *Nucleic Acids Res.* **2008**, *36*, 861–871.
- (47) Davin, L. B.; Bedgar, D. L.; Katayama, T.; Lewis, N. G. *Phytochemistry* **1992**, *31*, 3869–3874.
- (48) Huis, R.; Hawkins, S.; Neutelings, G. *BMC Plant Biol.* **2010**, *10*, 71.
- (49) Verwoerd, T. C.; Dekker, B. M. M.; Hoekema, A. *Nucleic Acids Res.* **1989**, *17*, 2362.
- (50) Gehrig, H. H.; Winter, K.; Cushman, J.; Borland, A.; Taybi, T. *Plant Mol. Biol. Rep.* **2000**, *18*, 369–376.
- (51) Marques, J. V.; Kim, K.-W.; Lee, C.; Costa, M. A.; May, G. D.; Crow, J. A.; Davin, L. B.; Lewis, N. G. *J. Biol. Chem.* **2013**, *288*, 466–479.